THE ASTROPHYSICAL JOURNAL, 284:211–222, 1984 September 1

THE MAGNETIC FIELDS OF THE LATE-TYPE STARS[1]

ERMANNO F. BORRA AND GEOFFREY EDWARDS
Département de physique, Observatoire du mont Mégantic, Université Laval

AND

M. MAYOR
Observatoire de Genève

Received 1984 January 3; accepted 1984 March 19

ABSTRACT

We have assembled a powerful stellar magnetometer capable of measuring longitudinal magnetic fields as small as a few gauss. Observations of known magnetic stars show that the instrument yields the expected values. A detailed study of the formal errors shows that they are realistic, although we cannot exclude that our most precise measurements may have errors that are twice as large as those claimed. We have observed a large number of late-type stars, and obtained mostly nulls or detections that are suspect. We do, however, find definite detections for the Ca II emission dwarf ξ Boo A and probable detections in the RS CVn star UX Ari. Observations of the transverse Zeeman effect do not show evidence of strong transverse fields, but our uncertainties are large (a few hundred gauss). We make an approximate estimate of the magnetic geometries of active dwarfs, concluding that the most likely geometry is complex and composed of several hundred patches of opposite polarities.

Subject headings: instruments — stars: late-type — stars: magnetic

I. INTRODUCTION

Surface magnetic fields are observable parameters of stars. They are, potentially, tracers of stellar structure and evolution like luminosities and effective temperatures. It is thus clearly of interest to study the incidence of magnetism among all main types of stars, throughout the H-R diagram. Magnetic fields have been detected among many types of stars. They have been measured with certainty in upper–main-sequence stars having peculiar spectra (see Borra, Landstreet, and Mestel 1982, hereafter BLM) and in white dwarfs (Angel 1978; Angel, Borra, and Landstreet 1981). These measurements have been mostly obtained with intermediate band (5 Å) circular polarimetry in the wings of Balmer lines for the upper–main-sequence stars and wide-band (>1000 Å) continuum polarization for the white dwarfs.

The situation is far less well defined among late-type nondegenerate stars. In those stars, the magnetic fields are detected in narrow spectral lines, either from line profiles or from polarization measurements in lines. The formal errors claimed in late-type stars are often smaller (by as much as a factor of 10) than those obtained in the upper–main-sequence stars. However, only a few detections have been claimed (BLM). These measures invariably have low signal-to-noise ratios and, often, later measurements of the same objects, made with greater precision, fail to confirm the claims. At the time of this writing, the only late-type star in which magnetic fields are known to be present with absolute certainty is the Sun.

There is, however, a growing body of evidence to indicate that magnetic fields of the order of 1000 gauss are present in many late-type stars. The pioneering work of Wilson (1978) has shown that many late-type stars display large and variable emission in the cores of Ca II H and K. Vaughan and Preston (1980) and Vaughan (1980) have pursued this line of work and have found that a substantial fraction of these stars show cyclic variations similar to the solar cycle. By analogy with the Sun, where intense Ca II emission is associated with regions of strong magnetic fields, one may assume that the strong Ca II emission observed in many late-type stars is indicative of the presence of strong magnetic fields over a substantial fraction of the surface of the star. Magnetic fields have also been inferred in various types of late-type stars from indirect evidence such as the presence of coronae, starspots (Dorren and Guinan 1982), and solar flares, which are associated with magnetic activity in the Sun. This has led to searches for magnetic fields in those stars. Robinson, Worden, and Harvey (1980) used a line-broadening technique developed by Robinson (1980) and found evidence for a surface field in ξ Bootis. Marcy (1984) carried out an extensive survey of magnetism among late-type stars and, using a line-broadening technique, claimed several detections. Detections using line-broadening techniques have also been claimed by Giampapa, Golub, and Worden (1981) for the RS CVn star λ And and by Gray (1984) in a sample of F, G, and K dwarfs. The magnetic fields inferred have strengths of the order of 1000 gauss in patches that cover of the order of 50% of the visible disk of the star.

In this work we extend considerably the magnetic exploration of the H-R diagram by carrying out a survey for magnetism among many groups of late-type stars. For this purpose we have assembled and tested a new powerful instrument, Coramag, that can measure the longitudinal or transverse components of the magnetic fields in bright sharp-lined stars with formal errors as small as 1 gauss.

II. CORAMAG, THE INSTRUMENT

The technique used is the same as the one described by Borra, Fletcher, and Poeckert (1981, hereafter BFP) (see also Brown and Landstreet 1981). We interfaced the polarizing optics and electronics of the Laval University Pockels cell polarimeter with Coravel, the Cassegrain echelle radial velocity spectrometer described by Baranne, Mayor, and Poncet (1979).

[1] Based on observations collected at the Haute-Provence Observatory.

The instrument issued from this union is called Coramag. A KD*P crystal, followed by a Glan-Thompson prism, is placed in front of the entrance slit of the spectrograph. During the first observing run (1981 November), the polarizing optics were placed directly in the converging beam (f/15) of the telescope. During the following runs a collimating lens was used, so that the optics operated in collimated light. The KD*P crystal is switched $\pm\lambda/4$ with high-voltage square pulses at a frequency of 100 Hz. In conjunction with the Glan-Thompson prism, this results in admitting alternately the left and right circular polarized components of the starlight into the spectrograph (at 100 Hz). For a more detailed and technical discussion of the technique applied to the measurements of stellar magnetic fields, see Borra (1980*b*). The advantage of this technique comes from the fact that the net polarization is measured as a difference in intensity between two otherwise identical beams, separated in time by 10 ms, with the same detector.

We first use the instrument in its radial velocity measurement mode and find the position at which the mask matches the stellar spectral lines. The photon counts from the photomultipliers are then routed to the photon counting electronics of the polarimeter. A calibrating circular polarizer is used to set the operating voltage of the Pockels cell at the beginning of the night. This calibration is checked whenever the temperature inside the instrument varies by a few degrees. Each observation of a star is always preceded and followed by observations through the circular polarizer, to insure that the instrument is operating properly. The mask is then positioned so that the slits admit the light from a chosen position on the lines or on the continuum. For example, in our search for longitudinal magnetic fields, our most common mode of operation, the slits are first positioned on the blue wings of the lines. The circular polarization is then measured (switching at 100 Hz) up to a predetermined number of counts, after which the circular polarization signal $v_b{}^1$ is recorded. The slits are then moved to the opposite (red) wings of the lines and counts are accumulated up to the same total number, yielding the $v_r{}^1$. The sequence continues in the order $v_b{}^1, v_r{}^1, v_r{}^2, \ldots, v_b{}^{n-1}, v_b{}^n, v_r{}^n$ giving after n pairs of integrations:

$$\langle V\rangle = \sum_{i=1}^{N} \frac{v_b{}^i - v_r{}^i}{2N} .$$

The procedure is thus similar to the one used by BFP, except that the counts are gathered to a predetermined number rather than a predetermined integration time. Coramag is used at the Cassegrain focus; hence, the starlight does not encounter any oblique reflection off metallic mirrors before reaching the polarizing optics. We do not have to worry about time-varying instrumental polarization. The instrumental polarization is very small and quite constant in time. BFP had to deal with time-varying instrumental polarization and needed fixed integration time intervals. Very small instrumental polarization is one of the advantages of Coramag over coudé polarimeters. Coramag is also a very efficient instrument. The careful optimization of Coravel for radial velocity measurements (Baranne, Mayor, and Poncet 1979) optimizes also the efficiency of Coramag as a magnetometer. The instrument, for example, observes 1500 lines simultaneously (from 4000 Å to 5000 Å) in two orders with a total of 3000 slits. The mask used is obtained from a spectrum of Arcturus (K2 III); it is thus optimized for a K2 III star. However, because most of the spectral lines used are Fe I lines, the mask is useful over a very large range of spectral types. For example, we can use it to observe Ap stars, as reported in the next section. This mask is the same as the one used for radial velocity measurements. It is very time consuming to make new masks as well as to interchange and align them. For this reason, we did not make a mask optimized for magnetic measurements. In any event, we are not sure that this would much improve the sensitivity of the instrument.

The instrument is also used to measure linear polarization inside spectral lines. A quarter-wave plate is swung into place in front of the Pockels cell. It transforms one of the Stokes parameters (e.g., Q) into circular polarization which is then measured by the polarimeter. The quarter-wave plate is then rotated by 45° to measure the Stokes parameter U. The wave plate can be positioned at 90° and 135° to give $-Q$ and $-U$. Each observation of a star is always preceded and followed by an observation through the linear polarizer as a check on the instrument. The linear polarization is obtained from $P^2 = Q^2 + U^2$ and the position angle from $\tan 2\theta = Q/U$. When the instrument is used to measure the transverse Zeeman effect, the slits are normally positioned in the center of the line, followed by observations in the wings. The slits can be positioned anywhere in the lines, and one can thus obtain the wavelength dependence of linear and circular polarization across the lines (Zeeman signatures). We have thus obtained Zeeman signatures in a few known magnetic Ap stars. The instrument can also be used to measure line broadening in the cross-correlation function.

III. REDUCTION TECHNIQUES AND OBSERVATIONS OF KNOWN MAGNETIC STARS

a) Observations of the Longitudinal Zeeman Effect

Let us consider a line formed in the presence of a homogeneous longitudinal magnetic field. A power series expansion of the line profile $I(\lambda)$, truncated after the first power term gives

$$V = 4.67 \times 10^{-13} z\lambda^2 B \frac{1}{I}\frac{dI}{d\lambda} , \qquad (2)$$

where V is the fractional circular polarization, z is the z-factor (Babcock 1962), λ is the wavelength in Å, and B is the longitudinal magnetic field in gauss. If the lines of force are inclined at an angle γ with respect to the line of sight, we can replace B with $B\cos\gamma$, the longitudinal component. In real stars, the magnetic field is not homogeneous, but numerical models (E. F. Borra, unpublished) show that, for simple magnetic geometries (such as a dipole) and weak fields (1000 gauss), this relation holds to a very good approximation provided $B\cos\gamma$ is replaced by the effective magnetic field B_e which is defined by

$$B_e = \int B\cos\gamma I dA \Big/ \int I dA , \qquad (3)$$

where the surface integrals are carried out over the visible disk of the star, I is local surface brightness, and dA is the local surface area element. We are observing several hundred lines simultaneously; hence the instrument measures

$$\langle V\rangle = 4.67 \times 10^{-13} B_e \sum_{i=1}^{1500} z_i \lambda_i{}^2 \frac{dI_i}{d\lambda} \Big/ \sum_{i=1}^{1500} I_i , \qquad (4)$$

where the sum is extended over all lines observed. This sum could be computed in principle, but this would clearly be an arduous task as the profiles of several hundred lines must be

obtained for every star observed. Moreover, this would be mostly an exercise in futility as the z-value of a given line is generally poorly known and z-values obtained from LS coupling are unreliable for heavy elements such as iron. Consider also that we are mostly interested in detections rather than exquisitely precise measurements and that, in any event, equation (2) is itself an approximation. To convert our polarization measures into magnetic field units we therefore use instead

$$\langle V \rangle = 4.67 \times 10^{-13} B_e \langle z \rangle \langle \lambda^2 \rangle < \left\langle \frac{1}{I} \frac{dI}{d\lambda} \right\rangle . \quad (5)$$

Using equation (5) eases greatly the reductions as $\langle 1/IdI/d\lambda \rangle$ is obtained directly from the crosscorrelation profile $\langle I(\lambda) \rangle$ which can be interpreted as an average line profile. The value of $\langle z \rangle$ is obtained by averaging z-values in the list of Babcock (1962) and in pages chosen at random in Sylvia Burd's extensive list of z-values (H. W. Babcock 1973, private communication). It is found that $\langle z \rangle = 1.30$, with very little scatter from page to page and about 30% scatter among individual z-values. The value of $\langle \lambda \rangle$ used is a function of spectral type (4200 Å to 4300 Å). Equation (5) is not rigorously exact, as the mean of a product is in general not equal to the product of the means. However, observations of known magnetic stars (Table 1 and Figs. 1 and 2; see also BFP) show good agreement between multislit measurements and measures obtained with other techniques. This is probably due to the small spread in z, λ and $1/IdI/d\lambda$ values among the lines. Equation (5) will thus be used in all reductions of circular polarization measures.

As a check on the technique and the instrument, we have observed three known magnetic Ap stars: β Coronae Borealis, 53 Camelopardalis, and γ Equulei. The measures obtained are presented in Table 1. We give, for every star, the Julian date at midpoint of observation, the $\langle V \rangle$ value obtained (eq. [1]) and its standard deviation, the B_e value obtained from $\langle V \rangle$ using equation (5) and the formal error associated with B_e. The standard deviation of $\langle V \rangle$ is computed under the assumption that photon shot noise is the only source of random error. Extensive use of the same analyzing optics and electronics (see BL and references therein) has shown that this is very nearly the case for polarization measurements. On the other hand, the error associated with B_e in Table 1 is the formal error obtained by converting the standard deviation of $\langle V \rangle$ into magnetic

TABLE 1

OBSERVATIONS OF LONGITUDINAL MAGNETIC FIELDS
(known magnetic Ap stars)

JD 2,440,000+	$\langle V \rangle \pm \sigma$ (%)	$B_e \pm \sigma$ (gauss)	B_e expected (gauss)	ϕ
		53 Camelopardalis		
4918.587.....	0.893 ± 0.053	3189 ± 190	3440	0.099
4920.615.....	1.247 ± 0.041	4110 ± 135	3125	0.351
4922.647.....	0.065 ± 0.029	304 ± 135	−3690	0.604
4923.703.....	−1.324 ± 0.036	−7365 ± 200	−4830	0.736
4924.663.....	−1.175 ± 0.034	−4753 ± 138	−3160	0.856
4925.657.....	−0.345 ± 0.050	−1462 ± 210	270	0.979
4926.556.....	0.652 ± 0.050	2370 ± 180	3270	0.091
5423.399.....	−0.586 ± 0.158	−2484 ± 670	600	0.990
		β Coronae Borealis		
5111.543.....	0.491 ± 0.013	652 ± 17	650	0.281
5113.428.....	0.365 ± 0.071	485 ± 94	580	0.382
5114.417.....	0.305 ± 0.032	405 ± 43	460	0.437
5116.506.....	0.0871 ± 0.032	116 ± 43	105	0.550
5416.613.....	−0.515 ± 0.050	−684 ± 66	−430	0.783
5420.618.....	−0.114 ± 0.038	−151 ± 50	−51	0.000
5427.559.....	0.405 ± 0.070	538 ± 93	591	0.375
		γ Equulei		
4916.267.....	−0.367 ± 0.0350	−414 ± 40	~ −400	...
4918.266.....	−0.389 ± 0.025	−440 ± 28	~ −400	...
4923.252.....	−0.327 ± 0.029	−368 ± 33	~ −400	...
5118.610.....	−0.391 ± 0.071	−440 ± 80	~ −400	...

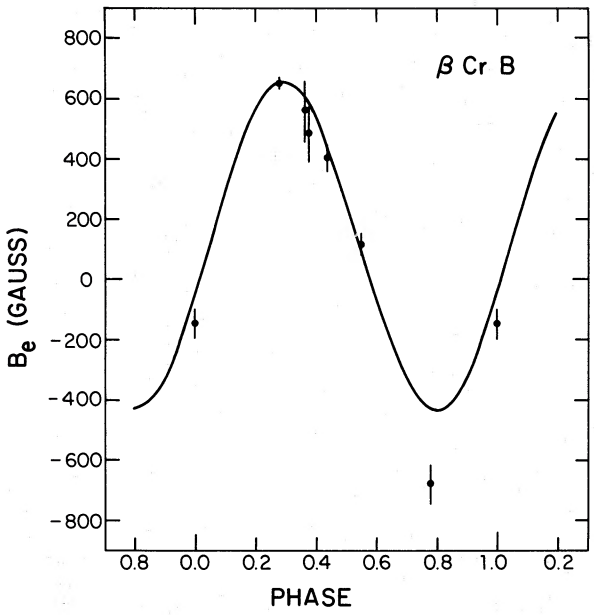

FIG. 1.—Our observations of the longitudinal magnetic field of the known magnetic star β Coronae Borealis are shown along with its known magnetic curve (*continuous line*). The error bars show the error ($\pm\sigma$) associated with each measurement.

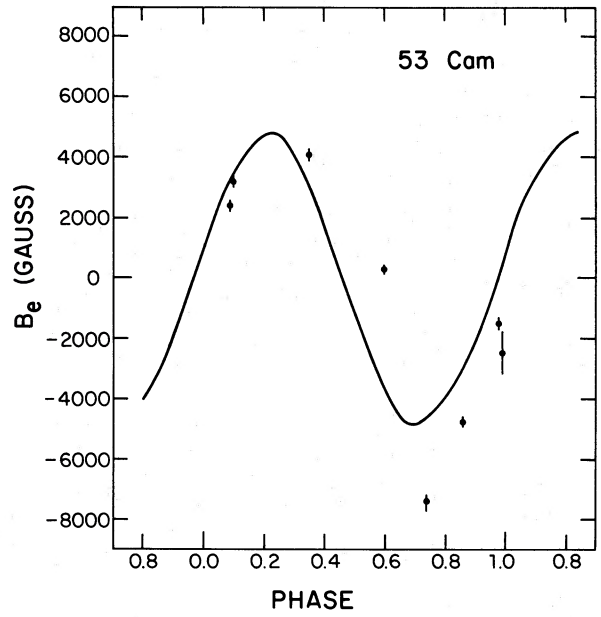

FIG. 2.—Our observations of the longitudinal magnetic field of the known magnetic star 53 Camelopardalis are shown along with its known magnetic curve (*continuous line*). The error bars show the error ($\pm\sigma$) associated with each measurement.

units via equation (5). This formal error, notwithstanding the fact that it is expressed in gauss for convenience, does not necessarily measure the whole uncertainty in B_e. It is, rather, a lower limit to this uncertainty as it only takes into account noise due to photon statistics. If a measurable magnetic field is present in the star observed, there is an additional uncertainty in converting the polarization measured into magnetic fields. *This fact is explained in what follows and must be understood before reading the rest of the paper.*

By using equation (5), we make the assumption that $V(\lambda)\alpha(1/I)\ dI/d\lambda$. This necessarily implies an S-shaped wavelength dependence. The validity of this assumption is, however, greatly model dependent. It depends on the strength of the magnetic field, the magnetic geometry of the star, and its rotational velocity as well as the inclination of the axis of rotation with respect to the line of sight (measured by $v \sin i$). All of these factors can cause $V(\lambda)$ to depart from the S-shaped profile predicted by equation (5). Our use of equation (5) is certainly valid for small fields ($B < 1000$ gauss) and small values of $v \sin i$ ($v \sin i < 1$ km s^{-1}). For stronger fields and small values of $v \sin i$, the validity depends on the magnetic geometry. If $v \sin i$ is greater than a few km s^{-1}, equation (5) may also give values of B_e grossly in error. The distortion of $V(\lambda)$ caused by rotational Doppler motions is the well-known crossover effect (Babcock 1960). Scans of $V(\lambda)$ across single spectral lines of magnetic Ap stars (Borra and Vaughan 1977, 1978; Borra 1980*b*) show examples of the complex Zeeman signatures that are present at times in magnetic stars. On the other hand, inspection of the scans presented in the above references shows that the same stars display at times the S-shaped profiles predicted by $1/I dI/d\lambda$. Computer models (E. F. Borra, unpublished) show that an S-shaped profile is produced, in a rotating star, whenever the visible disk has a geometry symmetric with respect to the rotation axis. This happens, for example, with a dipolar geometry where the axis of symmetry of the dipole is contained in the plane defined by the axis of rotation of the star and the line of sight. We can thus expect a star to give an S-shaped profile sometimes, while giving a complex profile at other times. This is illustrated in Figure 3 where we show the Zeeman signatures obtained with Coramag at two different magnetic phases of β CrB. A cross-correlation profile, which can be interpreted as an average line profile, is displayed below the polarization profiles. The scans were obtained by stepping the slits relative to the spectrum (actually, the slits are fixed and it is the spectrum that is moved). The observation obtained at phase 0.375, near positive extremum shows the simple S-shaped profile predicted by equation (5); we thus expect equation (5) to yield the correct value of B_e in that case. On the other hand, the scan obtained at phase 0.545, near crossover, where the field predicted is small (100 gauss), shows a profile quite different from the one predicted by equation (5). It is clear from this profile that the position of the slits in the blue and red wings is very critical as small changes in this position can change $(v_r^i - v_b^i)/2$ significantly. We can see from Figure 3 that the blue-wing red-wing sequence can yield zero field, a positive field, or a negative field, depending on the positions used. Consider that the working positions on the two wings are predetermined by eye on an oscilloscope display, in the presence of seeing and photon noise and, at times, on asymmetric line profiles; one can understand that the values of B_e obtained can differ systematically from the true values. On the other hand, after deciding where the blue red observations must be obtained, the slits are repositioned at

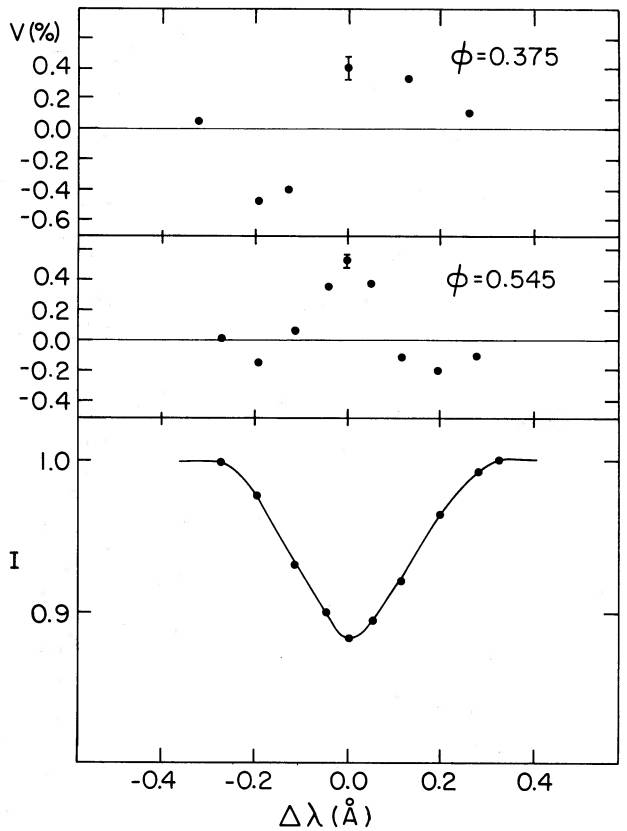

FIG. 3.—Scans of the circular polarization across the spectral lines of β CrB are shown for two selected phases of its magnetic cycle. The phases are indicated in the figure. Only one error bar ($\pm\sigma$) per scan has been plotted. All the measurements in a scan have the same precision. A cross-correlation profile (average line profile) is shown below the scans.

the same places during the sequence of red and blue wing observations. These individual observations last several minutes, the Pockels cell switching at 100 Hz.

This explains why, if (and only if) a detectable magnetic field is present, the formal error of $\langle V \rangle$ is a good measure of the uncertainty of $\langle V \rangle$, while the formal error quoted for B_e is not necessarily a good indication of the uncertainty of B_e. This is presumably the reason why the observation of phase 0.60 of 53 Cam gives such a discrepant value of B_e. 53 Cam shows a very conspicuous crossover effect and has very asymmetric line profiles. The slits were probably poorly positioned for that observation. In the search for magnetic fields presented in the next section, we will be interested primarly in detections rather than exact measurements; we are therefore not overly concerned with the effects discussed above.

The agreement between our observations of β CrB and the B_e curve from Borra and Landstreet (1980) is excellent with perhaps the exception of the observation near negative polarity. The negative extremum of this star has long been suspected to vary although this variation is not well established (see Borra and Landstreet 1980). We perhaps see that effect in Figure 1. This anomalous observation is also possibly due to the fact that the value of $dI/d\lambda$ used is inexact, either because we misjudged the positions of the slits or because of uncertainty in the line profile used. The agreement with 53 Cam is less satisfactory (Fig. 2 and Table 1). This is due in part to the uncertainty in the period of variation. We can clearly see

that a much better agreement can be achieved by shifting slightly the continuous line to the right by a few hundreths of a cycle. Such a shift is compatible with the uncertainties of the ephemeris (and the parameters of the sine curve) given by Borra and Landstreet (1980). Even then, however, some points would still be in less than perfect agreement with the magnetic curve determined by Borra and Landstreet (1980). This is probably due to the fact that the magnetic field of this star is very large and that the star shows a large crossover effect. Still, it is reassuring that, even for this star, the magnetic field obtained is usually near the expected value and never in gross disagreement with it. We have also several observations of γ Equulei. This star has a very long period of variation (several decades). We can see (Table 1) that our measurements repeat well from night to night (within the errors claimed) and are in full agreement with the measurements of Borra and Landstreet (1980) (who find a mean value of $B_e = -415$ gauss) and are also consistent with a very long period of variation.

b) *Observations of the Transverse Zeeman Effect*

It is well known that in an absorption line formed in the presence of a magnetic field, the Π component is linearly polarized with the electric vector perpendicular to the lines of force. The σ components are usually elliptically polarized, and the linear polarization component has its electric vector component parallel to the magnetic lines of force. If the magnetic field is purely transverse, the components are linearly polarized. This is the transverse inverse Zeeman effect. Observations of the linear polarization across the lines can thus yield additional information regarding the geometry of the magnetic field. In particular, some magnetic geometries (such as a dipolar field seen equator-on) can give a substantial amount of linear polarization but zero circular polarization. Observations of the linear polarization are thus useful complements to observations of the circular polarization.

Let us consider a line formed in the presence of a homogeneous transverse magnetic field. It can be shown that a power expansion of the line profile, truncated after the second power term gives

$$P = (4.67 \times 10^{-13} z \lambda^2 B)^2 \frac{1}{I} \frac{d^2 I^2}{d\lambda^2}, \quad (6)$$

where all the quantities are the same as in equation (2), P is the fractional linear polarization, and B is the transverse magnetic field in gauss. If the lines of force are inclined at an angle γ with respect to the line of sight, B can be replaced with $B \sin \gamma$. In a star having a complex geometry, B is then the averaged transverse magnetic field B_t given by

$$B_t = \int B \sin \gamma \sin 2\phi \frac{IdA}{\int IdA}, \quad (7)$$

where ϕ is an azimuthal angle, measured from the direction of the net polarization vector and the other symbols are the same as in equation (3). As we can see from equation (6), the polarization expected is $\propto d^2 I/d\lambda^2$ and to the square of the Zeeman splitting. We thus expect P to be smaller than V for small fields (about 1000 gauss), but on the other hand, because $P \propto B_t^2$ (from the Zeeman splitting), P can be comparable or larger than V for larger fields. $P(\lambda)$ will also show the crossover effect and the discussion concerning $V(\lambda)$ and our use of equation (8). The angle of the electric vector of polarization also gives the angle that B_t makes in the plane of the sky. We obtain the average transverse magnetic field from

$$B_t^2 = \frac{P}{(4.67 \times 10^{-13} \langle z \rangle \langle \lambda \rangle^2)^2} \frac{1}{I} \frac{d^2 I}{d\lambda^2}. \quad (8)$$

The quantities are the same as the ones in equation (5), and the same discussion again applies. $\langle 1/Id^2 I/d\lambda^2 \rangle$ is obtained by taking the second derivative of the cross-correlation profile. The value of P used in equation (8) is obtained from

$$P^2 = \{[(Q_b + Q_r)/2 - Q_c]/2\}^2 + \{[(U_b + U_r)/2 - U_c]/2\}^2 - \sigma_p^2, \quad (9)$$

where Q and U are the Stokes parameters and the subscripts b, r, and c indicate whether the Stokes parameter is measured in the wings or the core of the lines. The standard deviation σ_p is subtracted from the data because we take the squares of signed quantities that have random errors associated to them. We would overestimate systematically P^2 otherwise. Equation (9) is used because it removes the instrumental and interstellar polarization from the Zeeman polarization. On the other hand, by using equation (9) with equation (8), we give equal weight to the polarization from the wings and the core of the lines, while equation (6) shows that, for a given magnetic field, the polarization is proportional to the second derivative of the line profile. We find that, typically, the value of $d^2 I/d\lambda^2/I$ is 3 times as large in the center of the line than in the wings. The advantage of this procedure is that an error is introduced only if a magnetic field is detected. We are, in this work, interested primarily in detections rather than precise measurements; therefore, we adopt this reduction procedure which removes polarization of a nonmagnetic nature even through it introduces some calibration error in the magnetic field measured. We will not be overly concerned with the small error introduced, because we did not find any definite transverse magnetic field. Our main concern is to avoid spurious detections. The value of $\langle 1/Id^2 I/d\lambda^2 \rangle$ used is the geometric mean of the values in the core and in the wings. The calibration error introduced is small (about 10%).

We observe known polarization standards (Serkowski 1974) before we carry out a set of observations of the transverse Zeeman effect. These observations are used as a further check that the instrument is working properly, to calibrate its efficiency and to set the zero point of the position angle. A few stars having negligible interstellar polarization (Serkowski 1974) were also observed occasionally to determine the instrumental polarization; it was found to be negligible.

IV. OBSERVATIONS OF LATE-TYPE STARS: DISCUSSION OF THE RANDOM ERRORS

a) *Observations of the Longitudinal Zeeman Effect*

Table 2 lists our observations of circular polarization and, therefore, gives a summary of our search for longitudinal magnetic fields. The stars have been grouped by spectral type and luminosity class. We observed many normal late-type stars with the unique criterion that they be bright and accessible at the time of observation. We have also observed bright representatives of other types of stars because they have been suspected to be magnetic in the scientific literature. This is the case for Cepheids, RS CVn stars, dwarf emission stars, and G5 III giants.

The most noteworthy features of Table 2 are the very small standard deviations claimed for many bright stars and that

TABLE 2

OBSERVATIONS OF LONGITUDINAL MAGNETIC FIELDS

JD 2 440 000+	NAME	Sp. TYPE	V	σ_V	B	σ_B	s (nomag)	σ (ind)	s (mag)	N	REMARKS
					DWARFS (LUMINOSITY CLASS V)						
5294.564	α CMi	F5V	-0.0091	0.0071	-7.5	5.9	0.0128	0.0100		2	
5115.493	17 Cyg	F5V	0.0189	0.0177	20.0	19.0	0.0617	0.0500		8	CaIIem
*4920.569	π3 Ori	G0V	-0.0042	0.0091	-8.3	18.0	0.0258	0.0220		6	CaIIem
5293.333	61 Cyg	F7V	-0.0167	0.0748	-9.0	40.0	0.0189	0.0990		2	CaIIem
4918.548	χ Ori	G0V	0.0111	0.0242	9.5	21.0	0.0641	0.0630		4	CaIIem
*4925.589	χ Ori	G0V	0.0055	0.0077	4.7	6.6	0.0214	0.0230		8	
5293.589	χ Ori	G0V	-0.0017	0.0284	1.5	24.0	0.0025	0.0400		2	
*4922.433	η Cas	G0V	0.0002	0.0093	0.0	6.3	0.0149	0.0230		6	
5423.471	ξ UMaA	G0V	-0.0043	0.0287	-3.5	23.2	0.0488	0.0710		6	RSCVn
5423.495	ξ UMaB	G0V	-0.5258	0.3345	-425.0	271.0	0.7634	0.5000		2	1.6σ RSCVn
4918.426	κ Cet	G5V	0.0101	0.0288	5.5	15.7	0.0284	0.0710		6	CaIIem
4924.51	UX Ari	G5V	0.0593	0.0232	84.0	33.0	0.0798	0.0750	0.0685	10	2.6σ RSCVn
4925.456	UX Ari	G5V	0.0368	0.0211	52.0	30.0	0.0834	0.0710	0.0727	10	1.7σ
4926.389	UX Ari	G5V	0.0100	0.0289	14.0	41.0	0.0289	0.0710		6	
5293.385	UX Ari	G5V	-0.0297	0.0707	-42.0	100.0	0.0419	0.1000		2	
4920.376	τ Cet	G8V	-0.0087	0.0146	-5.0	8.5	0.0578	0.0410		8	CaIIem
4924.363	τ Cet	G8V	-0.0094	0.0117	-5.5	6.9	0.0376	0.0410		8	
5115.392	ξ BooA	G8Ve	0.0463	0.0118	25.0	6.4	0.0639	0.0500	0.0425	18	3.9σ CaIIem
5116.406	ξ BooA	G8Ve	0.0097	0.0145	5.2	7.8	0.0473	0.0500		12	
5118.458	ξ BooA	G8Ve	-0.0162	0.0134	-8.7	7.2	0.0380	0.0500		12	
5119.436	ξ BooA	G8Ve	0.1328	0.0552	72.0	30.0	0.2017	0.1070		2	2.4σ
5415.622	ξ BooA	G8Ve	0.0068	0.0225	3.7	12.1	0.1238	0.0710		10	
5416.523	ξ BooA	G8Ve	0.0687	0.0562	37.1	30.3	0.0927	0.0920		2	
5417.550	ξ BooA	G8Ve	0.0161	0.0193	8.7	10.4	0.2007	0.1920		4	
5419.625	ξ BooA	G8Ve	0.0052	0.0182	2.8	9.8	0.0901	0.1000		16	
5420.519	ξ BooA	G8Ve	0.0186	0.0249	10.0	13.4	0.0337	0.0710		4	
5423.630	ξ BooA	G8Ve	0.0190	0.0132	10.2	7.1	0.0614	0.1000		16	
5424.584	ξ BooA	G8Ve	-0.0063	0.0091	-3.4	4.9	0.0460	0.0500		16	
5429.493	HD105501	G8V	0.0004	0.0353	0.2	16.7	0.0597	0.1000		8	CaIIem
5428.653	12 Oph	K0V	-0.0569	0.0499	-22.0	19.0	0.2461	0.1580		10	CaIIem
5429.604	12 Oph	K0V	0.0040	0.0394	1.5	15.2	0.2119	0.2230		16	
5420.678	70 Oph	K0V	-0.0080	0.0249	-4.2	13.0	0.0448	0.0710		8	CaIIem
4922.465	o2 Eri	K1V	-0.0220	0.0151	-10.0	7.0	0.0447	0.0500		10	CaIIem
5293.526	o2 Eri	K1V	-0.0315	0.0320	-14.5	14.8	0.0442	0.0450		2	
4918.486	ε Eri	K2V	-0.0033	0.0165	-1.4	7.1	0.0423	0.0450		6	CaIIem
5291.507	ε Eri	K2V	0.0109	0.0249	4.7	10.8	0.0274	0.0500		4	
					GIANTS (LUMINOSITY CLASSES II - IV)						
5427.478	HR 5110	F2IV	0.0090	0.0223	15.0	36.0	0.0643	0.0710		10	RSCVn
*5425.493	η Boo	G0IV	-0.0062	0.0091	-5.6	8.2	0.0150	0.0180		4	
*5114.576	β Dra	G2II	-0.0041	0.0082	-2.2	4.4	0.0279	0.0250		8	mildly active
5419.520	β Crv	G5III	-0.0226	0.0190	-10.0	8.4	0.0522	0.0600		10	braking stage ?
5427.531	β Crv	G5III	0.0019	0.0322	0.8	14.3	0.0903	0.1120		6	
5423.533	93 Leo	G5III	-0.0093	0.0203	-11.0	24.4	0.1147	0.0710		10	RSCVn
5293.623	o UMa	G5III	0.0035	0.0100	1.3	3.8	0.0163	0.0200		4	braking stage ?
*5291.596	α Aur	G8III	0.0089	0.0025	9.2	2.6	0.0180	0.0071	0.0153	8	3.6σ RSCVn
*5294.417	α Aur	G8III	0.0021	0.0050	2.2	5.2	0.0137	0.0100		4	
*5416.343	α Aur	G8III	0.0108	0.0036	11.2	3.7	0.0237	0.0100	0.017	4	3.0σ
*5417.328	α Aur	G8III	-0.0048	0.0016	-5.0	1.7	0.0068	0.0020		2	3.0σ
5427.685	β Boo	G8III	0.0087	0.0266	3.1	9.5	0.0876	0.1000		10	
4922.295	λ And	G8III	-0.0050	0.0118	-2.4	5.6	0.0358	0.0290		6	
5420.483	ε Vir	G9II	-0.0094	0.0158	-3.2	5.4	0.0256	0.0320		4	
*4922.367	α Cas	K0II	0.0135	0.0068	4.3	2.2	0.0268	0.0230	0.0232	8	2.0σ
*4923.361	α Cas	K0II	-0.0043	0.0056	-1.4	1.8	0.0255	0.0160		8	
*5291.641	β Gem	K0III	0.0105	0.0064	3.3	2.0	0.0284	0.0160	0.026	6	1.6σ
*5419.347	β Gem	K0III	-0.0101	0.0047	-3.2	1.5	0.0209	0.0200		10	2.1σ
4920.515	δ Eri	K0IV	-0.0019	0.0144	-0.7	5.1	0.0284	0.0410		6	
4926.472	δ Eri	K0IV	0.0079	0.0103	2.8	3.7	0.0087	0.0220		4	
4920.690	σ Gem	K1III	-0.0143	0.0204	-23.0	32.0	0.0289	0.0410		4	RSCVn
5419.462	ψ UMa	K1III	0.0044	0.0288	1.4	9.2	0.0615	0.0710		6	
*4923.450	α Ari	K2III	-0.0066	0.0060	-2.0	1.8	0.0132	0.0150		6	
*5294.366	α Ari	K2III	0.0076	0.0070	2.3	2.1	0.0118	0.0140		4	
*5111.476	α Boo	K2III	-0.0010	0.0036	-0.3	1.1	0.0023	0.0071		4	
*5113.472	α Boo	K2III	0.0054	0.0041	1.6	1.2	0.0345	0.0100		6	
*5417.472	α Boo	K2III	0.0110	0.0017	3.3	0.5	0.0153	0.0020		2	6.5σ
*5428.542	α Boo	K2III	-0.0037	0.0050	-1.1	1.5	0.0152	0.0100		4	
4917.371	γ And	K3II	0.0222	0.0147	6.1	4.0	0.0248	0.0350		4	
*4920.439	γ And	K3II	-0.0064	0.0079	-1.8	2.2	0.0257	0.0230		8	
4915.610	ι Aur	K3II	0.0073	0.0124	1.9	3.3	0.0270	0.0350		8	
*5294.463	α Tau	K5III	-0.0028	0.0077	-0.8	2.1	0.0150	0.0180		4	
5425.435	α Lyn	M0III	-0.0037	0.0165	-1.1	4.8	0.0482	0.0500		8	
5419.423	μ UMa	M0III	-0.0134	0.0353	-4.0	10.5	0.1309	0.0710		4	
*5294.311	β And	M0III	-0.0002	0.0081	-0.1	2.4	0.0005	0.0160		4	
5114.507	δ Oph	M1III	-0.0033	0.0112	-0.9	3.2	0.0336	0.0224		4	
4916.349	β Peg	M2II	0.0062	0.0204	2.5	8.4	0.0239	0.0350		3	
*4926.651	μ Gem	M3III	0.0259	0.0057	9.1	2.0	0.0490	0.0230	0.041	16	4.5σ
5291.547	μ Gem	M3III	0.0205	0.0177	7.2	6.3	0.0271	0.0350		4	
5427.663	α Her	M5II	0.0022	0.0407	2.0	37.0	0.0834	0.1000		6	

TABLE 2—*Continued*

JD 2 440 000+	NAME	Sp. TYPE	V	σ_V	B	σ_B	s (nomag)	σ (ind)	s (mag)	N	REMARKS
					SUPERGIANTS (LUMINOSITY CLASS I)						
4918.364	δ Cep	F5I	-0.0015	0.0144	-1.6	15.3	0.0427	0.0410		8	Cepheid
*4921.268	δ Cep	F5I	-0.0036	0.0070	-1.7	3.4	0.0291	0.0290		14	
4923.284	δ Cep	F5I	0.0002	0.0354	0.2	31.8	0.0003	0.0500		2	
*4924.281	δ Cep	F5I	0.0016	0.0071	1.7	7.4	0.0316	0.0220		10	
*4925.474	δ Cep	F5I	0.0099	0.0057	6.5	3.8	0.0186	0.0180	0.0153	10	1.7σ
*4927.356	δ Cep	F5I	0.0200	0.0077			0.0366	0.0320	0.0296	12	2.6σ
*5294.307	δ Cep	F5I	0.0023	0.0094			0.0192	0.0200		4	
4926.260	HD180583	F6I	0.0049	0.0288			0.0273	0.0710		6	
5113.559	η Aql	F6I	0.0008	0.0100	1.1	13.3	0.0493	0.0316		10	Cepheid
5115.569	η Aql	F6I	-0.0176	0.0102	-13.3	7.7	0.0484	0.0500	0.039	12	1.7σ
4915.660	ζ Gem	F7I	0.0222	0.0157	9.5	6.7	0.0597	0.0500		10	Cepheid
4922.681	ζ Gem	F7I	-0.0225	0.0186	-13.2	10.9	0.0747	0.0710		6	
*4923.570	ζ Gem	F7I	0.0119	0.0062	6.4	3.3	0.0247	0.0270	0.0219	16	1.9σ
4918.301	χ Cyg	F7I	-0.0216	0.0576			0.1790	0.1410		6	Cepheid
*4916.312	γ Cyg	F8I	0.0071	0.0071	6.1	6.1	0.0242	0.0220		10	
4919.249	γ Cyg	F8I	0.0010	0.0130	0.9	11.0	0.0022	0.0230		3	
*4920.320	γ Cyg	F8I	-0.0053	0.0057	-4.6	4.9	0.0218	0.0160		8	
*4927.269	γ Cyg	F8I	-0.0024	0.0046	-2.1	4.0	0.0233	0.0110		6	
*5294.000	γ Cyg	F8I	0.0009	0.0063	0.8	5.4	0.0170	0.0130		4	
*4920.255	ε Gem	G8I	0.0024	0.0091	0.9	3.2	0.0194	0.0230		6	
*4926.333	Cep	K1Ib	0.0138	0.0079	4.5	2.6	0.0213	0.0220	0.015	8	1.7σ
*5294.517	α Ori	M2I	0.0155	0.0073	12.5	5.9	0.0265	0.0180	0.0203	6	2.1σ
*5424.337	α Ori	M2I	0.0146	0.0051	11.8	4.1	0.0265	0.0180	0.0302	14	2.9σ
*5425.348	α Ori	M2I	0.0131	0.0067	10.6	5.4	0.0326	0.0220	0.0269	6	2.0σ

very few detections are claimed, mostly marginal detections. The improvement with respect to photographic Zeeman observations is by nearly two orders of magnitude and one may therefore be surprised that we do not find many detections. On the other hand, if the Sun is typical of late-type stars, this is not surprising as complex and spotty magnetic geometries are expected to give small values of B_e.

Let us now turn our attention to the few detections in Table 2. A measure at three standard deviations is usually considered to be at the borderline for a legitimate claim and numerous detections at the two standard deviations level in a given object can also be interpreted as indicative of a real signal. The validity of our detections rests then on the trustworthiness of our formal errors. These errors are lower limits as they are derived on the basis of photon statistics. We must now prove that the formal errors claimed are not underestimates. Ideally, we should check the validity of our errors by observing null standards. Unfortunately, as measurements approaching this precision are rare (Borra, Landstreet, and Mestel 1982), there are simply no suitable magnetic null standards. We can, however, use the fact that the numbers in Table 2 are actually the mean of multiple measurements and also look at the distribution of measures in Table 2.

Coramag is actually a polarimeter, and a discussion of formal errors, especially when comparing observations of different stars having different line widths, should be concerned with polarization measures, rather than measures translated in magnetic units. We have divided our observations in Table 2 into two groups: a medium-precision group consisting of all measures having $\sigma \geq 0.01\%$, and a high-precision group having $\sigma < 0.01\%$. The high-precision measurements are identified with an asterisk in Table 2. We have plotted V/σ for the medium-precision group in Figure 4. If the errors claimed are realistic and most stars have undetectable magnetic fields, Figure 4 should be well fitted by a Gaussian with, perhaps, a long tail indicating real detections. The expected Gaussian distribution is shown by the continuous line in Figure 4. We can see that the medium-precision observations are well represented by a Gaussian distribution, with the exception of a single observation at $V/\sigma = 3.9$ (ξ Boo, Table 2). A χ^2 test from $V/\sigma = -2.2$ to $V/\sigma = 2.2$ gives reduced χ^2_ν value of 1.01 (44 degrees of freedom). The probability of exceeding 1.01 with 44 degrees of freedom is 0.40; this indicates that the standard deviations claimed for the medium-precision observations are consistent with the observations. The V/σ values for the high-precision observations have been plotted in Figure 5, where we have also plotted the expected Gaussian distribution (*continuous line*). We can see a poorer fit than in Figure 4. A χ^2 test, including the data from $V/\sigma = -2.2$ to $V/\sigma = 2.2$, gives a reduced χ^2 value of $\chi^2/\nu = 1.21$ (44 degrees of freedom). The probability associated with this χ^2/ν value is 0.1. This indicates either that the high-precision observations, as a group, tend to have random errors higher than the formal errors claimed or that a few marginal detections are present in the data.

The observations listed in Table 2 are actually averages of several individual measurements; the number N of measurements for each observation is indicated in the eleventh column of Table 2. This allows us to measure the actual scatter in the data, and we can compute the variance associated with each observation from

$$s^2 = \frac{1}{N-1} \sum_{i=1}^{N} (V_i - \bar{V})^2 \tag{10}$$

with

$$\bar{V} = \frac{1}{N} \sum_{i=1}^{N} V_i , \tag{11}$$

where V_i are the individual measurements and N is the total number of measurements. The variance s is thus a measure of the scatter around the instrumental polarization. If the longitudinal magnetic field of a given star is negligible and if the formal errors obtained from counting statistics are reasonable estimates of the noise, the s (nonmagnetic hypothesis) $\approx \sigma$

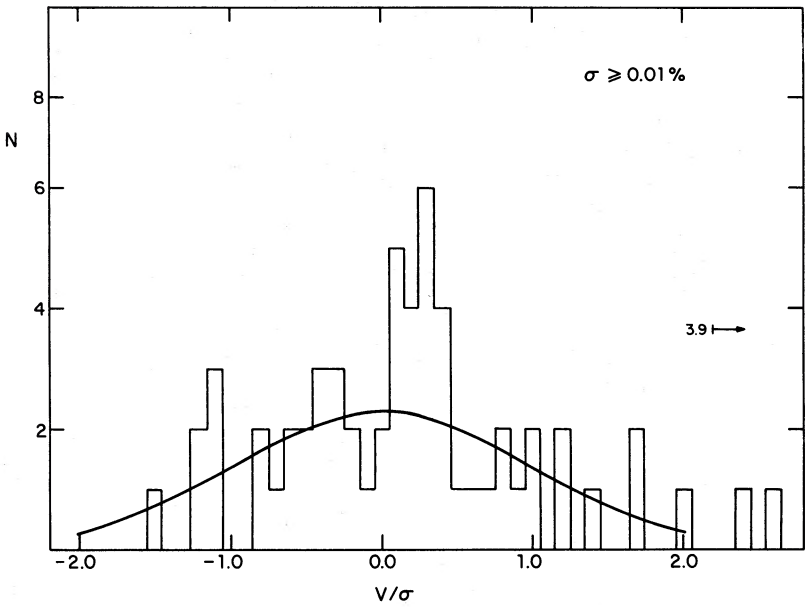

FIG. 4.—The histogram shows the distribution of V/σ (signal-to-noise ratio) for our medium-precision measurements ($\sigma \geq 0.01\%$). The arrow points to the position of a V/σ measure. The continuous line shows the distribution expected under the assumption that none of the stars are magnetic.

(individual) where σ (individual) is the formal error of an individual measurement. The values of s (nonmagnetic) and σ (individual) are displayed in the eighth and ninth columns of Table 2. We see that for most observations (in particular the medium-precision ones) s (nonmag) $\approx \sigma$ (indiv). We have also computed another value of the variance, for the observations having $V/\sigma > 1.5$, from

$$S = \frac{1}{N-1} \sum_{i=1}^{N} [(-1)^w V_i - \bar{V}) \tag{12}$$

$$\bar{V} = \frac{1}{N} \sum (-1)^w V_i , \tag{13}$$

where $w = 1$ or 2, depending on whether we observe the blue or the red wings. This value of s (magnetic hypothesis) measures the scatter under the hypothesis that a longitudinal magnetic field is present and that the circular polarization is antisymmetric with respect to the center of the line (S-shaped). The values of s (magnetic) are shown in the tenth column of Table 2. The values of s (magnetic) are smaller than s (nonmagnetic); in some instances s (magnetic) is $\leq \sigma$ (ind) while in others s (magnetic) $> \sigma$ (ind). Because s^2/σ^2 (ind) $= \chi^2/\nu$ with $N-1$ degrees of freedom (Bevington 1969), we can attach a quantitative significance level to σ (ind) in Table 2. By comparing the probabilities associated with $\chi^2/\nu = s^2/\sigma^2$ to the frequencies observed, one reaches the same conclusions reached

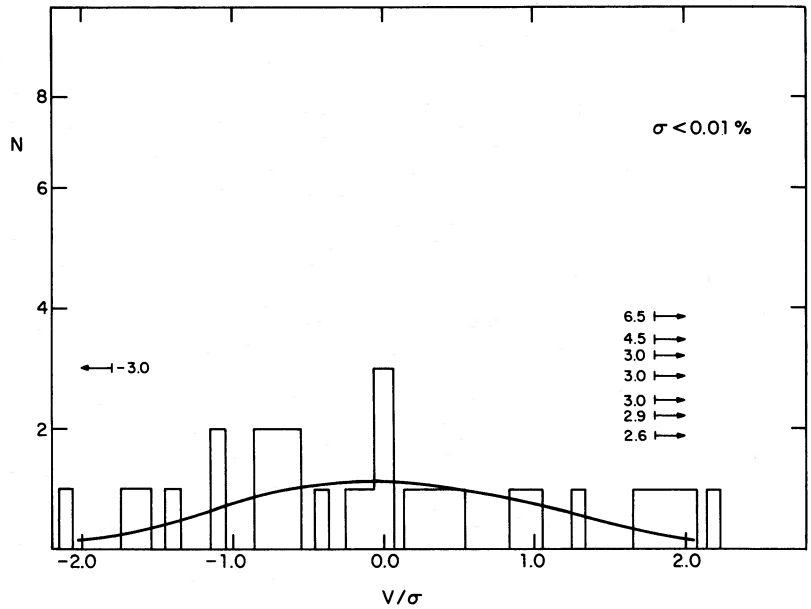

FIG. 5.—The histogram shows the distribution of V/σ (signal-to-noise ratio) for our high-precision measurements ($\sigma < 0.01\%$). The arrows point to the directions of several measurements that do not fit within the frame of the figure. The continuous line shows the distribution expected under the assumption that none of the stars are magnetic.

from the χ^2 tests of Figures 4 and 5: the formal errors of the medium-precision observations are consistent with the data, while the high-precision formal errors are not. This does not mean that all of the high-precision measurements should be rejected. The variances computed under the nonmagnetic hypothesis may be too large because magnetic fields are present and the variances computed under the magnetic hypothesis assume that the Zeeman signatures are antisymmetric. If Doppler motions (crossover effect) are important in those observations the Zeeman signature is not antisymmetric (see Fig. 3) and both s (nonmagnetic) and s (magnetic) will be abnormally large. We cannot therefore say conclusively whether the high-precision errors are reliable or not. We do not have a quantitative way of testing for presence of the crossover effect. This could be tested if we had observations at the center of the lines but, with a few exceptions, we do not have these observations.

It may be useful to summarize the error analysis with a conservative appraisal of the situation: the medium-precision observations are reliable, but the high-precision observations are suspect. The high-precision observations must be evaluated individually and s^2/σ^2 (ind) $= \chi^2/\nu$, with $\nu = N - 1$ degrees of freedom, gives a quantitative estimate of the reliability of each observation.

b) *Observations of the Transverse Zeeman Effect*

Our observations of the transverse Zeeman effect are shown in Table 3. We give the Julian date, the value of P (eq. [9]) and its standard deviation (computed under the assumption that the only source of error comes from photon counting statistics), and the 95% confidence level interval of B_t. These observations belong mostly to the medium-precision group ($\sigma > 0.01\%$), and we expect that the errors quoted are realistic. We do not have enough observations to carry out a good error analysis, but we can see that three observations out of 11 are above one standard deviation, as expected. We have one observation at the 2.6 standard deviation level (0.1 expected), possibly due to a real signal.

V. OBSERVATIONS OF LATE-TYPE STARS: DISCUSSION OF DETECTIONS

a) *Observations of the Longitudinal Zeeman Effect*

In the light of the discussion of errors in § IV we come to the conclusion that longitudinal magnetic fields have been discovered in ξ Bootis. This is shown by the 3.9 standard deviation measurement obtained at JD = 2,445,115.392. The probability that a 3.9 σ (or greater) observations arises from statistical fluctuations is 10^{-4}. We have 100 observations in Table 2 and would thus expect, statistically, 10^{-2} observations at the 3.9 σ level or greater. We have thus reasons to believe that we detected a real signal in ξ Boo, provided we did not underestimate σ. We have enough individual measurements ($N = 18$) on that night that we can obtain a very good comparison between the formal errors and the internal scatter of the data; we can see that the value of the variance under the magnetic hypothesis ($s = 0.0425\%$) is in complete agreement with the theoretical standard deviation [σ (ind) $= 0.025\%$]. Moreover, this observation belongs to the medium-precision group for which enough nulls have been obtained to give us faith in the few detections. The same star has a 2.4 σ detection at JD 2,445,119.486. Unfortunately, we have only two measurements on that night, and we cannot compute the variance. The detection of a magnetic field in this star is particularly interesting because ξ Boo belongs to the class of dwarf stars having strong emission in the cores of Ca II H and K. Magnetic fields have been claimed for many members of this class (Marcy 1984) including ξ Boo itself (Robinson, Worden, and Harvey 1980). These fields were detected with a line-broadening technique which measures the average surface field defined in equation (14). Table 2 shows that the longitudinal field of ξ Boo varied from 25 ± 6.4 gauss on JD 2,445,115.392 to 5.2 ± 7.8 gauss 24 hours later. This time scale is short compared to the period of rotation of the star (10 days). Such rapid changes have been seen in ξ Boo and other active stars (Baliunas *et al.* 1981; Marcy 1981). On the other hand, observational errors may account for a substantial part of the variations observed. We do not have detections for any of the other dwarf emission stars in Table 2.

It is also likely that UX Arietis is magnetic. This is shown by a 2.6 σ observation, followed by a 1.7 σ observation the next night. This star belongs to the RS CVn class. RS CVn stars have been suspected to have magnetic fields.

We have a few additional detections in Table 2. They all belong to the high-precision group and are therefore dependent on the reliability of the errors quoted. If we take the variance/standard deviation ratio and $s^2/\sigma^2 = \chi^2/\nu$ (with $N - 1$ degrees of freedom) as a measure of the reliability of the errors claimed, we see marginal detections in ζ Gem, δ Cep, η Aql, and α Ori. Given that we have 100 observations in Table 2, we can expect five measures at the 2 standard deviation level and one at the 2.6 standard deviation level; this can account for some of the marginal detections in Table 2. On the other hand, it is strange that we have a concentration of marginal detections among our observations of Cepheids. We see a measure at 2.6 σ and another one at 1.7 σ in δ Cep, one at 1.7 σ in η Aql, and one at 1.9 σ in ζ Gem. Borra, Fletcher, and Poeckert (1981) have claimed probable detections of magnetic fields in Cepheids, using the same technique. It is frustrating that we cannot give a firmer confirmation, for unfortunately these observations are at the limit of the capability of existing instrumentation. Increasing the precision by only a factor of 2 will require a major effort. To add to our frustration, we were limited by the fork mount of the telescope to declinations smaller than $+65°$, and we could not therefore observe α UMa, the star in which Borra, Fletcher, and Poeckert (1981) obtained their best detection.

It is puzzling that we obtain three detections at the 2–2.9 standard deviation level in α Orionis. The variances, especially the variances under the magnetic hypothesis, are in reasonable agreement with σ (ind) for these observations.

TABLE 3

OBSERVATIONS OF TRANSVERSE MAGNETIC FIELDS

JD 2,440,000+	Name	$P \pm \sigma$ (%)	B (95% confidence) (gauss)
5291.456.....	ϵ Eri	0.067 ± 0.026	(235,663)
5292.497.....	π^3 Ori	0.0106 ± 0.087	(0,2150)
5293.295.....	61 Cyg *B*	0.0 ± 0.0704	(0,800)
5293.425.....	UX Ari	0.0 ± 0.0702	(0,1400)
5293.486.....	o^2 Eri	0.0 ± 0.0312	(0,486)
5293.561.....	χ^1 Ori	0.036 ± 0.028	(0,895)
5293.671.....	o UMa	0.0155 ± 0.018	...
5420.569.....	ξ Boo	0.017 ± 0.027	(0,570)
5428.611.....	α Boo	0.00757 ± 0.0057	(0,220)
5429.466.....	ϵ Vir	0.0 ± 0.021	(0,322)
5429.519.....	HD 101501	0.0 ± 0.071	(0,730)
5429.542.....	β CrV	0.0056 ± 0.0706	(0,760)

The remaining detections are suspect. Either the variance is substantially greater than σ (ind), or we have only two observations and we have no check on the validity of the standard errors claimed.

b) Observations of the Transverse Zeeman Effect

We can see from Table 3 that the limits we can give to the transverse magnetic fields are very large, almost two order of magntitude larger than for the longitudinal fields (Table 2). This illustrates the difficulty of measuring the transverse Zeeman effect. Unfortunately, because P is proportional to B_t^2 and σ_ρ is proportional to the inverse of the integration time, it will be very difficult to obtain more accurate observations and decrease much the uncertainty of B_t, considering that the observations in Table 3 were obtained with integrations times between 1 and 2 hours.

We may possibly have detected a field in ϵ Eri, but a single measure at 2.7 standard deviations is not a conclusive proof.

We must conclude that we have not found any convincing evidence of the transverse Zeeman effect.

VI. THE MAGNETIC GEOMETRIES OF THE LATE-TYPE STARS

We must reconcile the fact that magnetic fields of the error of 1000 gauss have been claimed, with line-broadening techniques, for many of the stars in Table 2 (see references in § I) while the measurements in Table 2 seem, prima facie, to indicate much weaker magnetic fields. Line-broadening techniques measure the average surface field (eq. [14]), while our polarization techniques measure an average component of the magnetic field (eqs. [3] and [7]). Therefore, the fact that our observations imply magnetic fields two orders of magnitude smaller than those found with line-broadening techniques does not indicate a conflict of claims but, rather, sets constraints on the magnetic geometries. It indicates that the magnetic geometries of the late-type stars are probably complex and composed of many patches having different strengths, sizes, and orientations of the magnetic lines of force.

Let us consider a simple model: a star having a magnetic region that occupies a fraction of the visible disk of the star. We shall not worry about magnetic flux conservation because flux need not be conserved in the region as long as it is conserved over the entire surface of the star. Let us call B_r the average surface field of the region, given by

$$B_r = \frac{\int BIdA}{\int IdA} . \tag{14}$$

This is the average scalar field responsible for line broadening. Let us also assume for simplicity that the light intensity I is constant over the region and that B_r is built from the contributions of N patches having area A_i and homogeneous magnetic fields of strength B_i and longitudinal components $B_i \cos \gamma_i$. We can then write

$$B_r = \sum_{i=1}^{N} B_i A_i \Big/ \sum_{i=1}^{N} A_i \tag{15}$$

or

$$B_r = \sum_{i=1}^{N} B_i a_i \tag{16}$$

with

$$a_i = A_i \Big/ \sum_{i=1}^{N} A_i ;$$

in addition

$$B_e^r = \int B \cos \gamma \frac{IdA}{\int IdA} \tag{17}$$

which can also be written as

$$B_e^r = \sum_{i=1}^{N} B_i \cos \gamma_i a_i . \tag{18}$$

We can see that the average longitudinal field of the region is built from the contribution of N patches having different areas, strengths of polarities, and orientations. The mathematics of the situation is the same as the mathematics of a random walk of varying step sizes. The steps are $B_i \cos \gamma_i a_i$. Consequently, we have that

$$\langle B_e^r \rangle^2 = N \langle B \cos \gamma a \rangle^2 , \tag{19}$$

where $\langle B \cos \gamma a \rangle$ is the average "step size." Although the average of a product is not necessarily equal to the product of the average, we will write equation (19) as

$$B_e^r = \sqrt{N} \langle \cos \gamma \rangle \langle Ba \rangle \tag{20}$$

and therefore

$$B_e^r = \sqrt{N}/2 \langle Ba \rangle , \tag{21}$$

where $\cos \gamma$ has been averaged between 0 and $\pi/2$. This is also equivalent to assuming that all of the lines of forces in the patches are inclined at either $+60°$ or $-60°$ with respect to the line of sight. This approximation is not bad, if we considered that what will come out of this treatment will be an order of magnitude estimate of the number of patches in a typical magnetic late-type star.

Let us make another approximation, that $\langle Ba \rangle = B_r/N$; this is exact only if the region is made of regions of equal area and magnetic field strength, but it is not a bad approximation given our ultimate goal. Now we can write

$$B_e^r = \tfrac{1}{2} B_r / \sqrt{N} . \tag{22}$$

Our observation give B_e which is related to B_e^r by

$$B_e = B_e^r y f , \tag{23}$$

where y is the ratio of light intensities inside and outside the region and f is the fraction of the visible disk occupied by the magnetic region. We can then estimate the number of individual patches N that are present in the typical region of a typical star from

$$N = (B_r yf/2B_e)^2 . \tag{24}$$

In this analysis we have made the implicit assumption that the magnetic patches are concentrated in a single region. Indeed, there are indications that the stars have a small number of large regions. This is the only way the stars can produce the large light and Ca II emission variations that are observed (Vaughan *et al.* 1981; Dorren and Guinan 1982). On the other hand, equation (24) is also valid if the patches are distributed more or less uniformly across the star. The factor f is then a filling factor that takes into account the fraction of the visible disk occupied by the patches.

We can now estimate N. Observations (Marcy 1984) show that the average filling factor is about 0.5 for the most active stars and that the typical value of B_r is about 1000 gauss. Let us take $y = 0.8$. Table 2 is consistent with a typical value of the

order of 10 gauss or less. If we use $B_e = 10$ gauss and $B_r = 1000$ gauss, we see that $N = 400$. We can thus estimate that there are at least several hundred patches of negative and positive polarity in a typical magnetic late-type star.

This simple analysis can be extended to other models. We can assume, for example, that the patches are dipolar regions. We can then replace $B \cos \gamma$, in equation (17), with Bq, where q is the ratio between the longitudinal and surface fields in that patch. We then see that $N \propto \langle q \rangle^2$ (eq. [24]). This shows that the number of patches inferred is greatly dependent on the magnetic geometry of the patch. If $q = 0.05$, we can see that our observations are consistent with a very small number of patches (as small as one). It is thus conceivable that the late-type stars have starspots having the type of radial or azimuthal dipolar geometries discussed by Mullan (1979). The spots could then be detected by measures of the transverse Zeeman effect. It is frustrating that the detection limit of our observations of the transverse Zeeman effect are within a factor of 5 of what would be a useful limit. It is even more frustrating to know that more accurate measures will be very difficult to obtain. On the other hand one, must exercise care in using Mullan's models. His models compute the longitudinal, transverse, and surface fields with relations like those in equations (3), (7), and (14), but these quantities are not the ones that are actually measured; line and polarization profiles are the observed quantities. Borra (1974*a*, *b*) has shown that large systematic errors can result, from decentered dipole geometries of the type used by Mullan, when this fact is not accounted for. Although we have not modeled line profiles, we suspect that Mullan models suffer from this criticism.

VII. CONCLUSION

We have built a powerful instrument, Coramag, and we have shown that it is capable of measuring longitudinal magnetic fields of a few gauss. Observations of known magnetic Ap stars reproduce well their known magnetic curves, showing that there is no significant scaling error.

We have checked the reliability of our formal errors. It appears that measurements having polarization standard deviations $>0.01\%$ are consistent with the errors claimed. Higher precision measurements ($\sigma < 0.01\%$) are suspect as there seems to be excess noise. However, because these measurements tend to be also the most precise ones, after translation into magnetic units, it is possible that they appear excessively noisy because many of these stars have magnetic fields; indeed, most of these overly noisy observations indicate detections. We are, however, unable to affirm that these detections are trustworthy.

There is little doubt that a longitudinal magnetic field of a few tens of gauss has been discovered in the Ca II emission dwarf ξ Boo A. We are also reasonably confident that a magnetic field has been discovered in the RS CVn star UX Ari. Both types of stars were expected to be magnetic.

We have also observed several members of other classes of late-type stars, but we do not find any signal which is definite in terms of both signal-to-noise ratio and trustworthiness of the formal error claimed. For example, we did find significant signals in the RS CVn star α Aur; however, these high-precision measures are suspect, although we cannot exclude that they may be real. Although the few remaining detections are either marginal or suspect, they are tantalizing as they may show that we are at the limit of being able to measure the longitudinal components of the magnetic fields of many late-type stars. This would imply that many late-type stars have magnetic fields that are an order of magnitude larger than in the Sun.

Gray (1984) finds a dramatic drop in the rotational velocity of giant stars at spectral type G5 III. This he interprets as due to magnetic braking caused by a dynamo turning on and off again at that spectral type. We have observed two of Gray's stars (β CrV and o UMa), but we do not find evidence of magnetic fields. On the other hand, these stars are slow rotators, and the dynamo may have already been turned off.

We have carried out observations of the transverse Zeeman effect in a few stars (mostly Ca II emission dwarfs) but do not find any significant signal. The precision of these measurements is, however, much worse than for our measurements of longitudinal magnetic fields.

We used out upper limits (and detections) of the longitudinal magnetic fields of active dwarfs along with estimates of their surface fields (Marcy 1984) to gain some insight into the magnetic geometries of these stars. We conclude that the geometries are complex and probably consist of one (or very few) magnetic region composed of many patches (several hundred) of opposite polarities. These conclusions are, however, highly dependent on the magnetic geometries of the patches.

We wish to thank E. Ischi for his help in building Coramag and his assistance with the observations. This research has been funded by a National Sciences and Engineering Research Council of Canada grant to E. F. B. and by a Swiss National Sciences Foundation grant to M. M.

REFERENCES

Angel, J. R. P. 1978, *Ann. Rev. Astr. Ap.*, **16**, 487.
Angel, J. R. P., Borra, E. F., and Landstreet, J. D. 1981, *Ap. J. Suppl.*, **45**, 457.
Babcock, H. W. 1960, in *Stars and Stellar Systems*, Vol. **6**, *Stellar Atmospheres*, ed. J. Greenstein (Chicago: University of Chicago Press), p. 282.
———. 1962, in *Stars and Stellar Systems*, Vol. **2**, *Astronomical Techniques*, ed. W. A. Hiltner (Chicago: University of Chicago Press), p. 107.
Baliunas, S. L., Hartmann, L., Vaughan, A. H., Liller, W., and Dupree, A. K. 1981, *Ap. J.*, **246**, 473.
Baranne, A., Mayor, M., and Poncet, J. L. 1979, *Vistas Astr.*, **23**, 279.
Bevington, P. R. 1969, in *Data Reduction and Error Analysis for the Physical Sciences* (New York: McGraw-Hill).
Borra, E. F., 1974*a*, *Ap. J.*, **187**, 271.
———. 1974*b*, *Ap. J.*, **188**, 287.
———. 1980*a*, *Ap. J.*, **235**, 911.
———. 1980*b*, *Ricerche Astronomiche*, **10**, 35.
Borra, E. F., Fletcher, M., and Poeckert, R. 1981, *Ap. J.*, **247**, 569 (BFP).
Borra, E. F., and Landstreet, J. D. 1980, *Ap. J. Suppl.*, **42**, 421.
Borra, E. F., Landstreet, J. D., and Mestel, L. 1982, *Ann. Rev. Astr. Ap.*, **20**, 191 (BLM).
Borra, E. F., and Vaughan, A. H. 1977, *Ap. J.*, **216**, 462.
———. 1978, *Ap. J.*, **220**, 924.
Brown, D. N., and Landstreet, J. D. 1981, *Ap. J.*, **246**, 899.
Dorren, J. D., and Guinan, E. F. 1982, *A.J.*, **87**, 1546.
Gray, D. F. 1984, *Ap. J.*, **277**, 640.
Giampapa, M. S., Golub, L., and Worden, S. P. 1981, *Ap. J.* (*Letters*), **268**, L121.
Marcy, G. W. 1981, *Ap. J.*, **245**, 624.
———, 1984, *Ap. J.*, **276**, 286.
Mullan, D. G. 1979, *Ap. J.*, **231**, 152.
Robinson, R. D. 1980, *Ap. J.*, **239**, 961.

Robinson, R. D., Worden, S. P., and Harvey, J. W. 1980, *Ap. J. (Letters)*, **236**, L155.
Serkowski, K. 1974, in *Planets, Stars, and Nebulae Studied with Photopolarimetry*, ed. T. Gehrels (Tucson: The University of Arizona Press), p. 135.
Vaughan, A. H. 1980, *Pub. A.S.P.*, **92**, 392.
Vaughan, A. H., and Preston, G. W. 1980, *Pub. A.S.P.*, **92**, 385.
Vaughan, A. H., *et al.* 1981, *Ap. J.*, **246**, 473.
Wilson, O. C. 1978, *Ap. J.*, **226**, 379.

ERMANNO F. BORRA and GEOFFREY EDWARDS: Département de physique, Université Laval, Ste-Foy, Québec G1K 7P4, Canada

M. MAYOR: Observatoire de Genève, CH-1290 Sauverny, Switzerland